Sun *et al. Chem Synth* 2023;3:33
DOI: 10.20517/cs.2023.07

Chemical Synthesis

Review

Open Access

Advancements of non-viologen-based anolytes for pH-neutral aqueous organic redox flow batteries

Hong Sun[1,#], Feiyang Hu[2,#], Zirui Jiang[2], Zhiwen Cui[1], Mahalingam Ravivarma[2,*], Hao Fan[2], Jiangxuan Song[2,*], Duanyang Kong[1,*]

[1]State Key Laboratory of Chemical Resource Engineering, Beijing University of Chemical Technology, Beijing 100029, China.
[2]State Key Laboratory for Mechanical Behavior of Materials, Shaanxi International Research Center for Soft Matter, School of Materials Science and Engineering, Xi'an Jiaotong University, Xi'an 710049, Shaanxi, China.
[#]Authors contributed equally.

[*]**Correspondence to:** Prof. Duanyang Kong, State Key Laboratory of Chemical Resource Engineering, Beijing University of Chemical Technology, NO.15 of North Three-ring East Road, Chaoyang District, Beijing 100029, China. E-mail: kongdy@buct.edu.cn; Prof. Jiangxuan Song, State Key Laboratory for Mechanical Behavior of Materials, Shaanxi International Research Center for Soft Matter, School of Materials Science and Engineering, Xi'an Jiaotong University, No.28, West Xianning Road, Xi'an 710049, Shaanxi, China. E-mail: songjx@xjtu.edu.cn; Dr. Mahalingam Ravivarma, State Key Laboratory for Mechanical Behavior of Materials, Shaanxi International Research Center for Soft Matter, School of Materials Science and Engineering, Xi'an Jiaotong University, No.28, West Xianning Road, Xi'an 710049, Shaanxi, China. E-mail: ravivarma@xjtu.edu.cn

How to cite this article: Sun H, Hu F, Jiang Z, Cui Z, Ravivarma M, Fan H, Song J, Kong D. Advancements of non-viologen-based anolytes for pH-neutral aqueous organic redox flow batteries. *Chem Synth* 2023;3:33. https://dx.doi.org/10.20517/cs.2023.07

Received: 14 Feb 2023 **First Decision:** 15 Mar 2023 **Revised:** 6 Apr 2023 **Accepted:** 19 Apr 2023 **Published:** 4 Jul 2023

Academic Editors: Bao-Lian Su, Da-Gang Yu **Copy Editor:** Yanbing Bai **Production Editor:** Yanbing Bai

Abstract

Aqueous organic redox flow battery (AORFB) is regarded as the most promising next-generation technology for energy storage that stores electricity in redox-active organics lysed in mild salt-electrolytes. Composed of abundant elements such as C, H, O, and N, the adapted organics have a high degree of structural diversity and tunability, endowing it possible to modulate the physicochemical properties of water solubility, redox potential, and stability, and resulting in potential cost-effectiveness, ecological and environmental safety. Therefore, the designable organics consumedly expand the distance for exceeding battery behaviors in comparison with the inorganic counterparts. Herein, this study presents an overview of pH-neutral AORFBs that employ nonflammable water-soluble molecules with cheap inorganic salts as supporting electrolytes. Particular emphasis is given to the progress of molecular engineering design and synthesis of non-viologen-based organic anolytes and their respective AORFB performance. Additionally, some comments on present opportunities and perspectives of this ascendant domain are also demonstrated.

Keywords: Aqueous organic redox flow battery, pH-neutral, non-viologen derivatives, molecular engineering, stability mechanism

© The Author(s) 2023. **Open Access** This article is licensed under a Creative Commons Attribution 4.0 International License (https://creativecommons.org/licenses/by/4.0/), which permits unrestricted use, sharing, adaptation, distribution and reproduction in any medium or format, for any purpose, even commercially, as long as you give appropriate credit to the original author(s) and the source, provide a link to the Creative Commons license, and indicate if changes were made.

INTRODUCTION

With the achievement of consensus for carbon neutrality, energy transformation and upgrading, and energy structure modification have become the global active response to climate change and sustainable development[1]. Utilizing of clean energy such as wind- and solar- energy holds great foreground for solving the dilemma and realizing the harmonious development of humankind and nature[1,2]. However, their inherent characteristics of volatility, intermittence, and uncertainty bring non-negligible challenges to grid-connected systems[3]. Fortunately, energy storage technique allows flexible conversion among various energy types due to the advantages of high efficiency and reliability[4-6]. It is noteworthy that electrochemical energy storage guides a crucial direction for energy storage's primary development due to the features of modularization, fast response, and great potential for commercialization[7,8].

Over the past decades, electrochemical energy storage has successfully moved from a theoretical concept to practical applications, mainly including lithium-ion batteries, lead-carbon batteries, sodium-based batteries, and flow batteries[8-10]. Among these technologies, the redox flow battery (RFB) has attracted widespread attention with its unique decoupled power and energy design[11,12]. They can be utilized over a wide power scope (0.02-50 MW), long lifetime (5,000-13,000 cycles), and nonsticking discharge duration (0.01-10 h) with strengths of high-safety and flexible scale in large-scale energy storage field[13,14]. The most well-developed system to date is vanadium redox flow battery (VRFB), which can store and release energy through the change of vanadium valence states in the electrolyte, thereby less affecting electrolyte cross-contamination. However, the wide implementation for large-scale grid storage of VRFB may be limited by several shortages involving the restricted supply of V_2O_5 (\$24 kg^{-1}), highly corrosive electrolyte solutions (> 1 mol L^{-1} H^+), low energy density (E_d < 50 Wh L^{-1}), and sluggish redox kinetics (~10^{-6} cm s^{-1})[15,16].

Recently, aqueous organic redox flow battery (AORFB), as an emerging alternative to VRFB, leverages the reversible reactions of sustainable and water-soluble organics[15,17]. The past few years have witnessed the evolution of AORFB, such as high-power acidic/alkaline[18-20] and high-voltage neutral[21,22] systems, which are categorized by the acidity and alkalinity of different supporting electrolytes for organics. The remarkable neutral system exhibits safety, affordability, and green benefits, which resulted from applying non-corrosive and non-flammable electrolytes with low-cost inorganic salts (e.g., NaCl)[15,17]. Moreover, the neutral condition can effectively inhibit the side-reactions such as hydrogen/oxygen evolution, and acid/base involved- or catalyzed-chemical decay of active organics [Figure 1], which are usual-sighted in acidic/alkaline AORFBs. To date, neutral systems have exhibited much more stable battery performance and stood for the state-of-the-art of AORFBs[15,17,23].

The hinge of AORFBs is the redox-active organic, which is readily accessible and inexpensive on account of consisting of extensive elements (e.g., C, H, O, N). Importantly, the molecular structures are greatly tailorable and diverse, permitting adaptability in redox potential, solubility, chemical/electrochemical stability, and electrode reaction kinetics[13,24,25].

In recent years, evident advance has been achieved in molecular engineering design for electrolytes of AORFBs. Presented candidates are mainly focused on ferrocene (Fc)[21,26], quinone[19,27], viologen (Vi)[22,28-30], phenazine[31-33], phenothiazine[34], 2,2,6,6-tetramethyl-1-piperidinyloxy (TEMPO)[22,35-39], azobenzene[40], and alloxazine[41,42]. The TEMPO, Fc, and Vi derivatives are commonly used as catholytes and anolytes in neutral AORFBs due to their suitable redox potentials and intrinsic chemical/electrochemical stability. Especially, Vi derivatives are easy to solubilize (>1.0 M) in aqueous electrolytes as anolytes and can undergo a two-

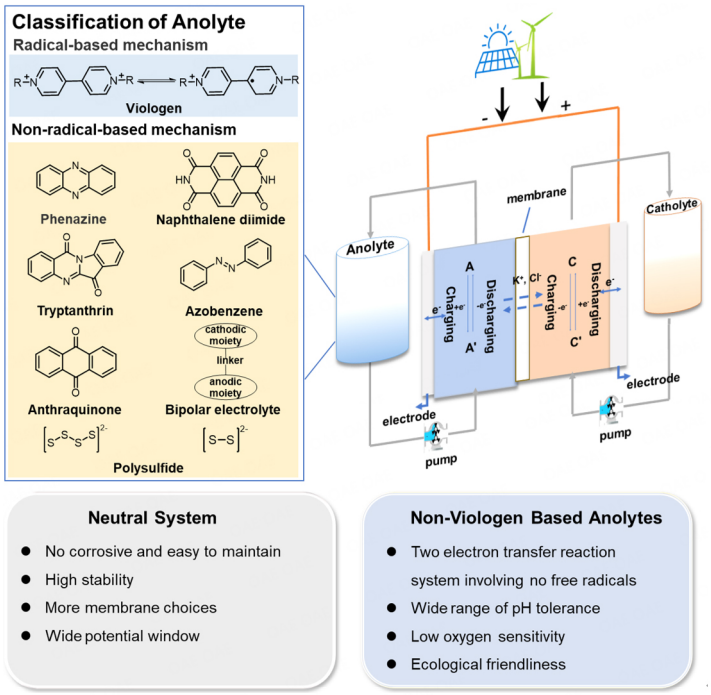

Figure 1. Schematic of a typical neutral RFB, classifications of anolyte, and the corresponding advantages in the neutral system and non-viologen-based anolytes. RFB: redox flow battery.

electron transfer process involving radical intermediates [Figure 1]. In particular, the insoluble nature of 2e reduction product Vi^0 with electrical neutrality in aqueous limits the full use of Vi (restricted utilization of the 2nd electron). Additionally, the oxygen-sensitive radical intermediate Vi^{+-} is subject to bimolecular decomposition or oxygenation, particularly under high concentration, leading to irreversible capacity decay[17,22,25,27-29]. In this review, we concentrate on the development of non-Vi-based anolytes in the neutral AORFB system, paying close attention to molecular engineering strategy of non-Vi organic species and their behaviors in whole battery operation. The latest progress in designed anolytes (negative electrolytes) and bipolar electrolytes was mainly summarized. In addition, the opportunities and perspectives of this burgeoning research field were outlined.

Figure. 1 shows a general scheme of an AORFB. Anolyte and catholyte flow through the electrochemical cell simultaneously by the pumps to proceed electrochemical reactions. In the charging process of the AORFB, C^- is oxidized to C, losing one electron which is driven to the other half cell where it reacts with A, reducing it to A^-. The C and A^- are the charged species in the system. Energy is stored by the reduction of anolyte and oxidation of catholyte; in the discharge process, the stored energy is outputted by the re-oxidation of anolyte and re-reduction of catholyte. During the charge/discharge process, anions or cations of the supporting electrolyte or counter ions of redox-active species act as charge carriers to cross through the separator to balance the charge of anolyte and catholyte.

NON-VIOLOGEN ANOLYTES FOR PH-NEUTRAL AORFBS

N-heterocyclic compounds anolytes

Due to the two-electron storage advantage and unique redox behavior, N-heterocyclics have been applied in pH-neutral AORFBs, such as phenazine (AFP), naphthalene (NDI) and tryptanthrin (TRYP). The N-heterocyclics structure has excellent stability, but the low water solubility and the chemical instability of its

derivatives limit its application and development. It has been shown that solubility can be increased by grafting water-soluble groups and the search for new N-heterocyclics is an effective way. In addition, to lower the reactivity and stabilize the radical, introducing redox-active pyridiniums to extend the conjugation is also a useful strategy. The philosophy of the design is to pioneer a dense electron-storage unit (triazine) and three radical stabilization units (pyridinium) which can increase the number of electron transfers and improve molecular stability.

Phenazine-based AORFBs

Phenazine-based derivatives are suitable candidates for anolytes in AORFBs with the main features of low redox potentials(~-0.6 V *vs.* SHE) [Table 1] and capable 2e transfer process[25]. In 2020 Ji *et al.* investigated a series of amino acid-functionalized phenazines (AFP) in near-neutral conditions[41]. Both acidic carboxyl and amino groups are suitable hydrophilic portions that could enable phenazines to have a higher solubility of about 1.0 M in water [Table 1].

As shown in Figure 2A, the compounds were synthesized via a one-step Pd-catalyzed Buchwald-Hartwig cross-coupling reaction of brominated phenazines and massive amino acids such as alanine, glycine, β-alanine, and γ-aminobutyric acid in the presence of 1%-2% palladium catalyst with high yields (84%-99%). The yield was desirable, which reflected less generation of waste and offered an effective synthesis.

When matched with $K_4[Fe(CN)_6]$ catholyte, the phenazine-based AORFBs exhibited high battery voltage and volumetric capacity because of introducing the amino acid groups [Figure 3A]. It was found that the substituted positions of amino acid groups played a key role in the battery's operational lifetime. In particular, β-Alanine modified 1,6-DPAP in AORFB displayed steady stability with no obvious capacity deterioration, which is more stable than 2,7-DPAP [Figure 3B]. Furthermore, CV tests in Figure 3C showed that the tautomer *tr*-2,7-DPAP had lost its reversibility in contrast with 2,7-DPAP, reflecting a rapid capacity fade in the battery. Other organics of 2,7-AFPs and 1,8-DGAP exhibited similar attenuation behaviors. DFT calculations of the tautomerization energy (ΔG) showed that ΔG from the reduced 1,6-DPAP (*re*-1,6-DPAP) to the tautomer (*tr*-1,6-DPAP) is 11.442 kJ mol^{-1} compared to -2.728 kJ mol^{-1} for ΔG from *re*-1,7-DPAP to *tr*-1,7-DPAP, corroborating that the reduced state for the former is more preferred [Figure 3D]. By pairing 1,6-DPAP anolyte with $K_4[Fe(CN)_6]$ catholyte at pH = 8 with 1.0 M electron transfer concentration, this AORFB exhibited an OCV of 1.15 V and a capacity of around 170 mAh at 20 mA cm^{-2}, as well as a record-low capacity decay rate of 0.000002%/cycle or 0.0015%/day [Table 1]. The results emphasize the great potential of amino acid functional groups to regulate redox-active organics in AORFBs.

Lately, Liang *et al.* developed 2,4,6-tris[1-(trimethylamonium)propyl-4-pyridiniumyl]-1,3,5-triazine hexachloride $[(TPyTz)Cl_6]$ as a reversible six-electron storage electrolyte by introducing a dense electron-storage unit (triazine) and three radical stabilization units (pyridinium)[43]. The synthetic protocol generally includes several steps in Figure 2B, as below. 4-cyanopyridine was used as the starting material to access 2.4.6-tri(4-pyridyl)-1.3.5-triazine (TPT), which is a key skeleton of the final product. Cyclization, a couple of ammoniations and three anion exchange processes afforded the desired product $(TPyTz)C_6$ in 24% yield over six steps. Obviously, the multistep reaction reduced the whole efficiency of the synthesis process. Although the synthesis steps for the molecule are complex, the reversible multi-electron transfer electrolyte is more advantageous in terms of high battery capacity and high energy density.

Electrochemical measurements revealed that $(TPyTz)Cl_6$ has a reversible 6e storage by four processes, and the former 4e storage was feasible under the operating conditions in a full battery [Figure 3E]. In addition, the CV curve in Figure 3F revealed three reversible redox processes, verifying the multi-electron transfer

Table 1. Summary of molecular physicochemical properties for non-Vi based redox-active organics and their applications in neutral AORFBs

Battery anolyte/catholyte with concentrations (M)	E (V *vs.* NHE)	k_0 ($\times 10^{-3}$ cm s^{-1})	D ($\times 10^{-6}$ cm^2 s^{-1})	S_{max} (M) (pH = 7)	OCV (V)	EE (%) at J_2(mA cm^{-2})	E_d (Wh L^{-1})	P_d (mW cm^{-2})	C_{rr} (%/cycle or day)	Ref
AADA/$K_3[Fe(CN)_6]$+$K_4[Fe(CN)_6]$ 0.1/NA	-0.79, -0.29	0.485	3.21	0.12 in H_2O	1.06,0.56	NA	NA	NA	99.95%/cycle	[39]
1,6-DPAP/$K_3[Fe(CN)_6]$+$K_4[Fe(CN)_6]$ 0.5/0.05+0.3	-0.56	0.513	4.08	1.005 in H_2O	1.15	NA	NA	NA	99.9985%/day	[40]
(TPyTz)Cl_6/FcNCl 0.3/0.11	-0.25, -0.44, -0.63	15, 6.5, 5.9	2.4, 2.4, 2.2	NA	0.88, 1.07, 1.26	72% at 40	NA	273	NA	[43]
2H-NDI/BTMAP-Fc 0.05/0.05	-0.28, -0.62	NA	1.9	NA	0.67	83% at 10	NA	NA	NA	[44, 45]
[K_2-BNDI]/4-HO-TEMPO 0.025/0.1	-0.20, -0.47	2.7, NA	3.95, 1.95	0.167 in H_2O 0.03 in KCl	1.0, 1.27	86% at 5	NA	37	99.958%/day	[46]
TRYP-SO_3H/BQDS 0.005/0.005	-0.46	0.362	0.0698	0.12 in KCl	0.94	67% at 5	0.07	NA	98% after 40 cycles	[48]
Lawsone/4-OH-TEMPO 0.1/0.2	-0.7	0.813	6.10	NA	1.3	74% at 10	NA	NA	99.992%/cycle	[49]
AQ-1,8-3E-OH/$K_3[Fe(CN)_6]$+$K_4[Fe(CN)_6]$ 1.5/0.31+0.31	-0.43	6.1(4)	2.94	2.24 in H_2O	1.0	84% at 50	25.2	180	99.5%/day	[51]
2,6-DPPEAQ/$K_3[Fe(CN)_6]$+$K_4[Fe(CN)_6]$ 0.1/0.01+0.1	-0.47 (unbuffered) -0.39 (buffered)	NA	1.37	0.75 (pH = 9)	1.0	NA	20.1 (theory)	160	99.99964%/cycle 99.986%/day	[52]
AQDS$(NH_4)_2$/NH_4I 0.75/0.75	-0.2	77	4.55	1.90 in H_2O	0.865	70.6% at 60	12.5	91.5	No decay after 300 cycles	[53]
PEG12-AQ/$K_4[Fe(CN)_6]$ 0.1/0.35	-0.64	2.236	15.9	Miscible with H_2O	0.847~1.01	87.6% at 20	1.8	120	99.67%/day 99.998%/cycle	[54]
2,7-AQDS/$K_4[Fe(CN)_6]$ 0.1/0.3	~-0.5	NA	NA	0.30 in KCl 0.80 in KCl with EG	0.76	81% at 40	NA	NA	> 99% until 100 cycles	[55]
1-DPAQCl/FcNCl 0.1/0.4	-0.562~ -0.700	4.92~ 23.0	3.63	1.44 in H_2O	1.11	~70% at 40	17.8~29.7	134	NA	[56]
QAAQ/FcNCl 0.2/0.4	-0.62	3.02	3.94	1.40 in H_2O 1.20 in NaCl	1.06	65% at 60	NA	33	99.959%/cycle	[57]
1,8-BDPAQCl_2/Fe(gly)$_2Cl_2$ 0.4/0.9	-0.755	-0.695	2.99	~1.07 in H_2O	1.27	61.3% at 40	NA	42.2	0.048%/cycle 0.88%/day	[58]
TEMPO-Phenazine Combi-molecule 0.01	-0.6, 0.6	3.99	2.35	NA	1.20	NA	NA	NA	No decay after 1800 cycles	[59]
RIBOTEMPO Combi-molecule 0.003	-0.72, 0.51	7.92, 5.39	7.54, 4.75	0.32 in KCl 1.22 in H_2O	1.23	NA	7.03, 26.81	NA	99.47%/cycle	[60]
Na_2S_2/$K_3[Fe(CN)_6]$ 1.0/1.0	-0.45, -0.7, -0.82; -0.46, -0.11	NA	NA	2.40 in H_2O	0.91	80% at 10	NA	NA	99.98%/cycle	[61]
K_2S/$K_3[Fe(CN)_6]$ 1.0/0.2	-0.51	NA	2.8	8.0 in KCl	0.97	80.95% under 34A	208 (theory)	153.4~ 213.9	99.979%/cycle	[62]

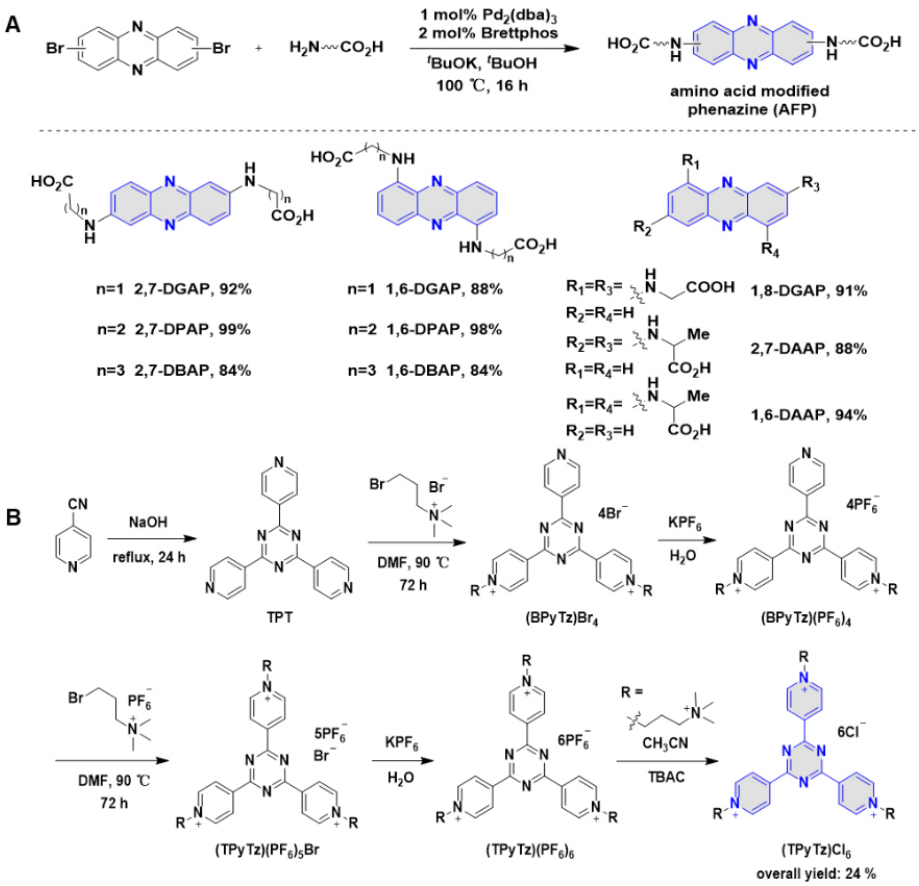

Figure 2. Synthesis schematic diagrams for phenazine-based derivatives. (A) Amino-acid functionalized phenazines; (B) Synthesis protocol of (TPyTz)Cl_6.

capability of the molecule. Subsequently, the assembled AORFB provided a specific capacity of 33.0 Ah L^{-1} and a peak power density of 273 mW cm^{-2} [Table 1]. This organic with multiple redox centers has a higher battery capacity and energy density than other molecules whose electron transfer capability is generally restricted to either 1e or 2e. This multi-electron storage control strategy will pave the way to exploit manageable and energy-dense AORFBs.

Naphthalene diimide-based AORFBs

Naphthalene diimide (NDI) possesses electrochemical stability and a 2-electron transfer process, as well as an inclusive chemistry ascription to the broad space for tuning its electronic properties by chemical substitution on the core unit. However, NDI is almost insoluble in water and has self-association properties[44,45], which limits its application in the field of RFBs. Fortunately, these problems are expected to be improved by selection of the side chain, which originates from imide nitrogen in the core structure. In contrast, its self-associative and solubility properties can be modified by selection of the side chain, which originates from imide nitrogen in the core structure. Such molecules have been entirely used in the field of polymer solar cells on account of their controllable electronic properties and good chemical stability[44].

In 2020, Medabalmi *et al.*reported a hydrophillic NDI derivative using Na- and K- salts of dicarboxylate as a new class of two-electron anolytes [Figure 4A][46]. The synthesis concerned a two-step process, in which N,N'-bis(glycinyl)naphthalene diimide (H_2BNDI) was first prepared and then converted into the

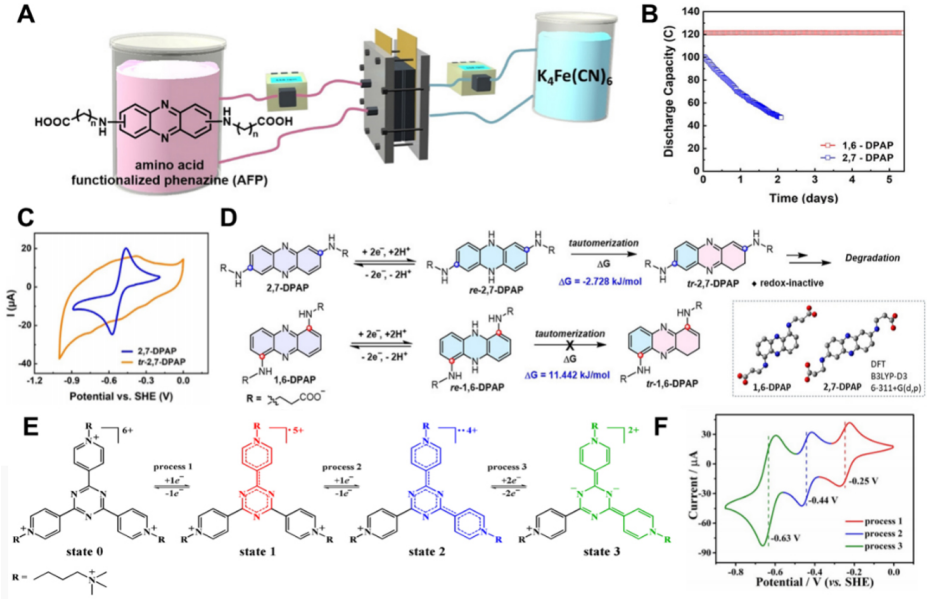

Figure 3. Performance for phenazine-based AORFBs[41,43]. (A) An assembled AORFB with AFP anolyte and ferrocyanide catholyte; (B) Discharge stability of 1,6-DPAP and 2,7-DPAP. Reproduced with permission[41]. Copyright 2020, Wiley-VCH; (C) CV curves of 2,7-DPAP and tr-2,7-DPAP. Condition: 1 M KCl at pH 12. Scan rate: 20 mV s^{-1}. Tr-2,7-DPAP was obtained from the reduced state after 10 days; (D) Proposed tautomerization pathway; (E) Schematic representation of the structural evolution of $(TPyTz)Cl_6$; (F) The corresponding CV curves. Condition: 4.0×10^{-3} M $(TPyTz)Cl_6$ in 0.5 M KCl. Scan rate: 50 mV s^{-1}. Reproduced with permission[43]. Copyright 2021, Wiley-VCH.

corresponding salts (K_2-BNDI or Na_2-BNDI) by treating with K_2CO_3/Na_2CO_3 in ethanol and water mixture. The synthesis process was easily conducted with a high yield of > 90% from inexpensive precursors.

As illustrated in Figure 4B, the CV curve of K_2-BNDI showed two stepwise transfers of single electron with redox potentials of -0.20 (c_1/a_1) and -0.47 V (c_2/a_2) *vs.* NHE [Table 1], correlated to the redox pairs of [K_2 BNDI]/[K_2-BNDI]$^{1-}$ and [K_2-BNDI]$^{1-}$/[K_2-BNDI]$^{2-}$, respectively. The remarkable two reversible processes were stable and reproducible with the results of repeating CV scans 500 times and the current density for both redox couples was enlarged as the scan rates increased. Subsequently, two types of M_2-BNDI (M = K or Na) anolyte performances were assessed in the full batteries paired with 4-OH-TEMPO catholyte. The result showed that compared with K_2-BNDI, the AORFB capacity density was more elongated with Na_2-BNDI anolyte, giving ~1.2 Ah L^{-1} at 10 mA cm^{-2} and ~0.8 Ah L^{-1} at 20 mA cm^{-2} [Figure 4C]. Furthermore, 40 mM Na_2-BNDI based AORFB presented improved stability and coulombic efficiency (CE) over 200 cycles [Figure 4D]. It is worth mentioning that the ^{1}H NMR and ESI-MS measurements revealed no decomposition evidence from the organics [Figure 4E], highlighting that electrochemical stability can be accessed from NDI-based anolytes. However, in order to meet the requirements of practical applications, the water solubility of the molecule (0.167 M in H_2O) still needs to be improved.

Later, in 2021, Ahlberg *et al.* investigated the operation of core-unsubstituted, N,N'-bis(dimethylaminopropyl)-NDI (2H-NDI) or N,N-bis(dimethylaminopropyl)-2,6-bis(dimethylamino)-NDI (2DMA-NDI) as anolyte in AORFBs[44]. The products are simply prepared in the mixture of 1,4,5,8-naphthalenetetracarboxylic dianhydride, 3-(dimethylamino)-1-propylamine, and water at 0 °C and then filtered through celite at room temperature under N_2 for 40 h. Accordingly, three AORFBs coupling 2H-NDI with 1,10-bis[3-(trimethylammonio)propyl] ferrocene dichloride (BTMAP-Fc) were demonstrated with varying performance levels. However, the best behavior was obtained from the core-substituted

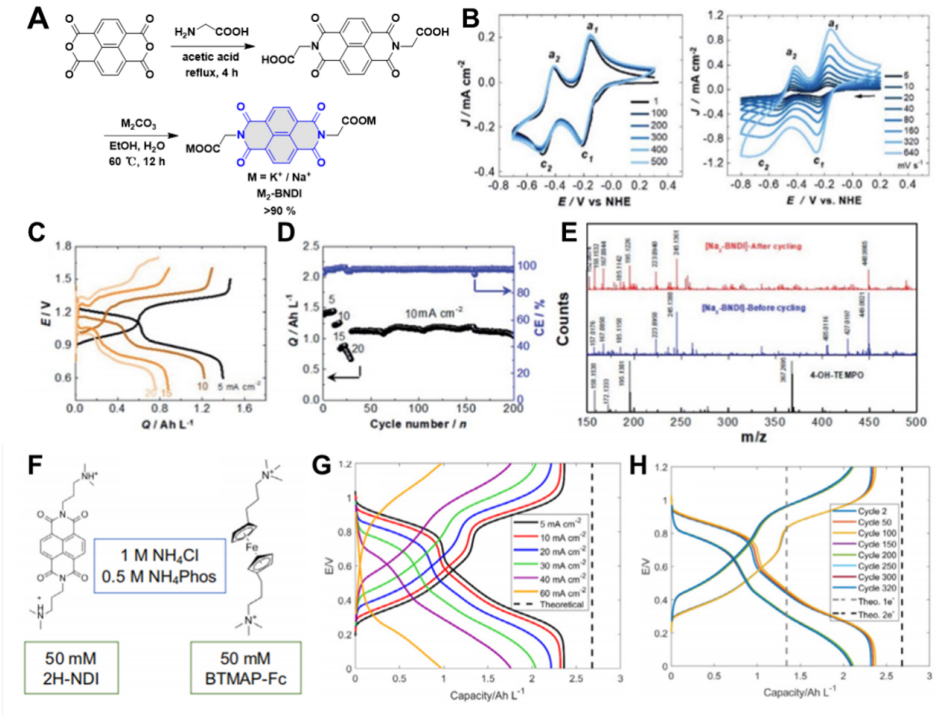

Figure 4. Naphthalene diimides (NDI) based derivatives and the performance for AORFBs[44,46]. (A) Synthesis of [M_2-BNDI] (M = K or Na); (B) CV curves of 5 mM [K_2-BNDI] in 1 M KCl for 500 cycles at 20 mV s^{-1} (left) and at scan rates from 5 to 640 mV s^{-1} (right); (C) Galvanostatic cycling profiles. Current density: 5-20 mA cm^{-2}; (D) Capacity retention and CE profiles for 200 cycles; (E) ESI-MS analysis with the positive ionization mode of [Na_2-BNDI] anolyte after 200 cycles (top). The as-prepared [Na_2-BNDI] (middle) and 4-OH-TEMPO (bottom) are presented for comparison; (F) An AORFB with 50 mM 2H-NDI and BTMAP-Fc in 0.5 M NH_4Phos and 1 M NH_4Cl; (G) Rate performance. Current density: 5-60 mA cm^{-2}. (H) Stability behavior. Reproduced with permission[46]. Copyright 2020, Royal Society of Chemistry.

dimethylamino-NDI (2DMA-NDI) anolyte. For 2H-NDI and 2DMA-NDI, a surprising increase in charge/discharge stability was presented when substituting K^+ from NH_4^+ as a cation.

The assembled 50 mM 2H-NDI/BTMAP-Fc AORFB in 1 M ammonium chloride and 0.5 M ammonium phosphate (NH_4Phos) was displayed in Figure 4F. The two obvious plateaus shown in Figure 4G and H, correspond to the two-electron transfer process. Besides, it was indicated from Figure 4G that the battery capacity regularly reduced as the current density increased. Furthermore, no capacity degradation was observed within 100 cycles and only a small amount of capacity decay (from ~2.3Ah/L to ~2.1Ah/L) occurred over 320 cycles, which suggests the good stability of the battery [Figure 4H]. For future development, the NDI molecules demand core-substituted to restrict self-association, and should take the selection of cation type for electrolyte into consideration, as well as the terminal groups that can enhance the solubility[44].

Tryptanthrin-based AORFBs

Tryptanthrin (TRYP) based derivatives are an astonishing family of biological/pharmacological compounds with the addition of showing fascinating redox properties because of the electron-accepting effect. TRYP demonstrates two reversible behaviors with respective cathodic and anodic peaks, stating that two 1e transfer processes are good candidates for anolytes in AORFBs[47] .

Marta *et al.* presented a sulfonated tryptanthrin (TRYP-SO_3H) through electrophilic aromatic substitution with neat chlorosulfonic acid at 60 °C for 48 h under N_2 atmosphere provided a dark green solid[47]. The ^{1}H NMR result confirmed that the substitution occurred at the 8- or 2-position of TRYP. After hydrolysis of TRYP-SO_3Cl, the tryptanthrin sulfonic acid derivatives including two isomers, TRYP-8SO_3H and TRYP-2 SO_3H, could be obtained [Figure 5A]. Two single AORFBs were constructed to study the performance of TRYP-SO_3H/$K_4[Fe(CN)]_6$ and TRYP-SO_3H/BQDS in neutral conditions [Figure 5B]. CV curves in Figure 5C indicated an expected OCV of 0.73 V for the TRYP-SO_3H/$K_4[Fe(CN)_6]$ AORFB, which was comparable to anthraquinone-2,7-disulfonic acid (0.76 V) in similar media. However, there was an apparent decrease in energy density for the organometallic redox couple TRYP-SO_3H/$K_4[Fe(CN)]_6$ during 50 cycles or ~7 h [Figure 5D]. By contrast, the all-organic redox couple TRYP-SO_3H/BQDS achieved a higher OCV of 0.94 V in comparison with $K_4[Fe(CN)_6]$ [Figure 5E and Table 1]. And more importantly, the CE steadily increased in ~10 cycles and further stabilized in 50 cycles (~29 h) [Figure 5F]. Overall, the all-organic TRYP-SO_3H/BQDS demonstrated a significantly improved lifetime with CE of 89% and energy efficiency (EE) of 67% as well as stable charge/discharge profiles during 29 hours [Table 1].

Quinone derivatives anolytes

Quinone and its derivatives store charges by an "ion-coordination" mechanism in which C = O groups are reduced to produce oxygen anions that are coordinated by guest cations. Quinones have been applied in pH-neutral AORFBs, such as naphthoquinone (NQ) and anthraquinone (AQ). However, the low solubility and chemical degradation restrain its application and development. Therefore, extensive research efforts have been devoted to improving solubility and chemical degradation. Adding polar functional groups (e.g., -OH, -COOH, -SO_3H, -PO_3H_2, *etc.*) and the selection of electrolyte counter-cations have been shown to tune the solubility of quinone and its derivatives. Last, using an ethylene glycol additive micellization strategy also can increase the solubility. At the same time, molecular engineering strategy can mitigate the chemical degradation caused by nucleophilic attacks. The micellization strategy improves stability by protecting the redox-active anthraquinone core in a hydrophilic poly (ethylene glycol) shell and increases the overall size to mitigate the crossover issue.

Naphthoquinone-based AORFBs

In 2018, Lin *et al.* developed a renewable biomolecule derived from natural henna, lawsone, as a stable AORFB anolyte [Figure 6A][48]. It possessed good reversibility with a relatively low redox potential of -0.7 V (*vs.* Ag/AgCl), which is an extremely low value among anolytes in AORFBs. In addition, facile alkalization with KOH further optimized its physicochemical properties. By coupling with 4-HO-TEMPO catholyte, the manufactured AORFB exhibited an extraordinary OCV of > 1.30 V [Figure 6B and Table 1]. As the state-of-charge (SOC) increased from 10% to 100%, the corresponding OCV increased from 1.22 to 1.33 V [Figure 6C]. Typical charge/discharge curves were plotted in Figure 6D with obvious plateaus, confirming that the two electrolytes undergo reversible reactions. Moreover, the measured discharge voltages were all above 1.15 V [Figure 6E]. Meanwhile, the battery showed stable performance with a capacity retention rate of 99.992%/cycle, CE of ~94%, and EE of ~74% [Figure 6F, 6G and Table 1].

Anthraquinone-based AORFBs

Anthraquinone (AQ) has extended p-conjugated structures in comparison with benzoquinones and naphthoquinones. Consequently, AQ owns more negative redox potential, less chance of crossover, higher chemical stability, and enriched structural versatility. Presently, AQ-based derivatives have become the primary anolytes in AORFBs and are acknowledged for their aforementioned advantages[49].

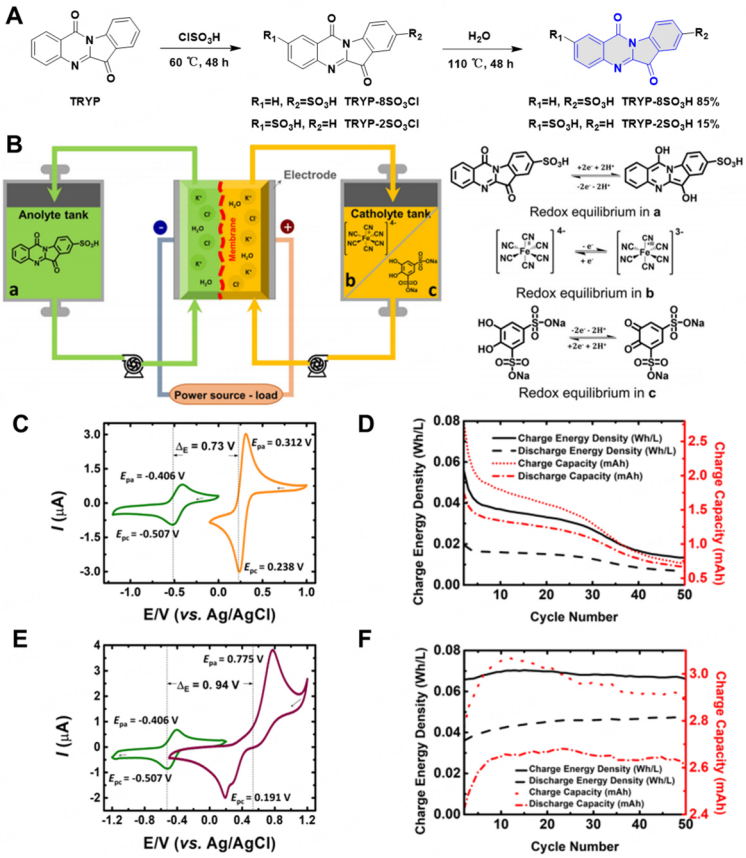

Figure 5. TRYP-based derivatives and the performance for AORFBs[47]. (A) Synthesis of TRYP-SO_3H; (B) Schematic illustration of an AORFB. Aqueous organometallic and all-organic battery using TRYP-SO_3H and $K_4[Fe(CN)_6]$/BQDS in neutral pH, and the corresponding redox mechanisms of TRYP-SO_3H, $K_4[Fe(CN)_6]$, and BQDS. (C, E) CVs at 50 mV s^{-1} in 1.0 M KCl of C: 1.0 mM TRYP-SO_3H (green trace) + 1.0 mM $K_4[Fe(CN)_6]$·(orange trace) and E: 1.0 mM TRYSO_3H (green trace) + 1.0 mM BQDS (purple trace); (D, F) Charge-discharge energy density and charge-discharge capacity plots of neutral pH aqueous organometallic and all-organic materials for AORFBs using 5.0 mM of TRYP-SO_3H in 1.0 M KCl as anolyte and (D) 10.0 mM of $K_4[Fe(CN)_6]$·or (F) 5.0 mM of BQDS as catholyte.

In 2019, Aziz *et al.* synthesized a series of PEG-substituted anthraquinones (PEGAQs) and carefully investigated an isomer, namely, 1,8-bis[2-(2-(2-hydroxyethoxy)ethoxy)ethoxy]anthracene-9,10-dione (AQ-1,8-3E-OH) [Figure 7A][50]. The compounds were synthesized with a high-temperature reaction procedure, dissolving *n,m*-dihydroxy-anthraquinone (DHAQ), anhydrous K_2CO_3, NaI, and 2-[2-(2-chloroethoxy) ethoxy] ethan-1-ol in DMF. The concentrated mixture was then extracted by DCM, dried over Na_2SO_4, purified by silica gel chromatography, and labelled as *n,m*-di-Pegylated AQ.

AQ-1,8-3E-OH is capable of miscible with water, thus exhibiting a high capacity of 80.4 Ah/L and energy density of 25.2 Wh/L for the battery with a concentration of 1.5 M at pH 7. To further study the performance of the water-miscibility anolyte, an AORFB was fabricated with a concentrated anolyte comprising 7 mL 1.5 M AQ-1,8-3E-OH in 1 M KCl as the capacity-limiting side and catholyte comprising 150 mL 0.31 M $K_4Fe(CN)_6$-$K_3Fe(CN)_6$ in 1 M KCl as the non-capacity-limiting side. Polarization experiments conducted at different SOCs of AQ-1,8-3E-OH indicated the maximum peak power density of 0.17 W cm^{-2} at near 100% SOC [Figure 7C]. In addition, the OCV improved from 0.96 to 1.20 V as the SOC increased from 10% to 90% [Figure 7D]. Upon electrochemical cycling during 220 cycles over 18 days, the battery displayed a temporal decay rate of 0.5%/day with an average current efficiency of 99.9%

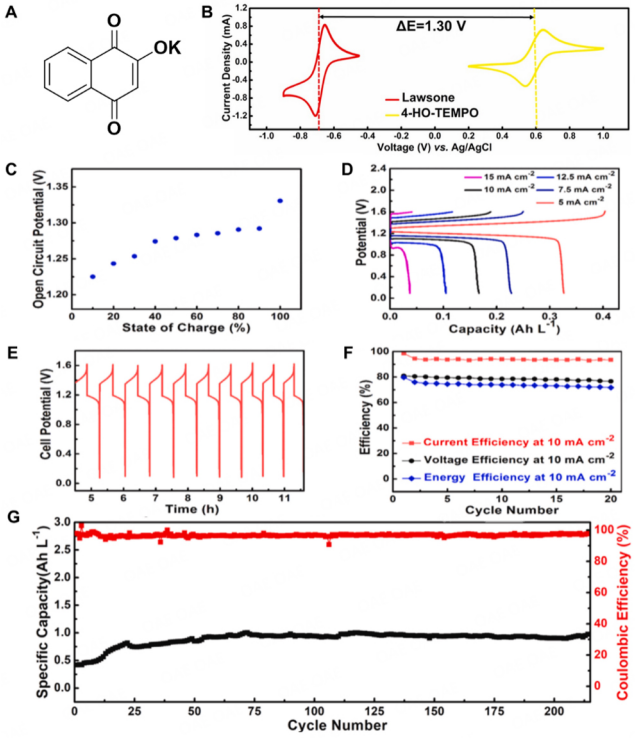

Figure 6. Electrochemical performance of lawsone-based AORFBs[48]. (A) Structure of lawsone-K; (B) CV curves of 0.01 M lawsone (red curve) and 0.02 M TEMPO (yellow curve). Scan rate: 50 mV s^{-1}; (C) OCVs versus SOCs; (D) Voltage profiles concerning battery capacity. Current density: 5-15 mA hcm^{-2}; (E) Constant-current cycling and (F) battery efficiencies. Current density: 10 mA cm^{-2}; (G) Long cycle performance of 0.1 M lawsone. Current density: 15 mA cm^{-2}. Reproduced with permission[48]. Copyright 2019, Elsevier.

[Figure 7E and Table 1].

Then, Aziz *et al.*furthered the research on AQ-based anolyte by developing a stable phosphonate-modified AQ anolyte which presented many advantages that can be used for scalable industrial manufacturing [Figure 7B][51]. The general synthesis process consisted of two steps with the reactions of O-alkylation and ester hydrolysis. The main purpose of this strategy is to introduce the water-soluble phosphonic acid groups. As a result, it achieved a high solubility at pH = 9 and above as well as steady stability at both pH = 9 and 12. CV curves of 2,6-DPPEAQ showed a redox peak at -0.47 V *vs.* SHE in pH = 9 unbuffered solution and at -0.49 V *vs.* SHE in pH = 12 unbuffered solution [Figure 7F]. In addition, the OCV and peak power density of a 2,6-DPPEAQ full battery against a $K_4Fe(CN)_6/K_3Fe(CN)_6$ catholyte were 0.95 V and 0.06 W cm^{-2} at 10% SOC, and 1.05 V and 0.16 W cm^{-2} at 90% SOC, respectively, which is close to AQ-1,8-3E-OH. Remarkably, the battery presented a low capacity fade rate of 0.00036%/cycle or 0.014%/day during 480 cycles [Figure 7G and Table 1].

One means of increasing the solubility of organics is by improving the type of ions in equilibrium. Liu *et al.* reported AQDS-$(NH_4)_2$, a diammonium salt, as an anolyte to pH-neutral AORFBs with high solubility in water [Figure 8A][52]. Through two steps, the desired product can be obtained with high yields. The Na^+-salts were transformed to AQSH and $AQDSH_2$ via an amberlite cation exchange resin. When the counter-cation Na^+ was replaced by NH_4^+, the hydrophilicity of the ammonia and hydrogen bonds formed between NH_4^+ and AQDS anion facilitated the dissolution of the salt, and thus the solubility and chemical stability were enhanced [Figure 8C]. Upon performing the CV of the aforementioned molecules, the curves in Figure 8D

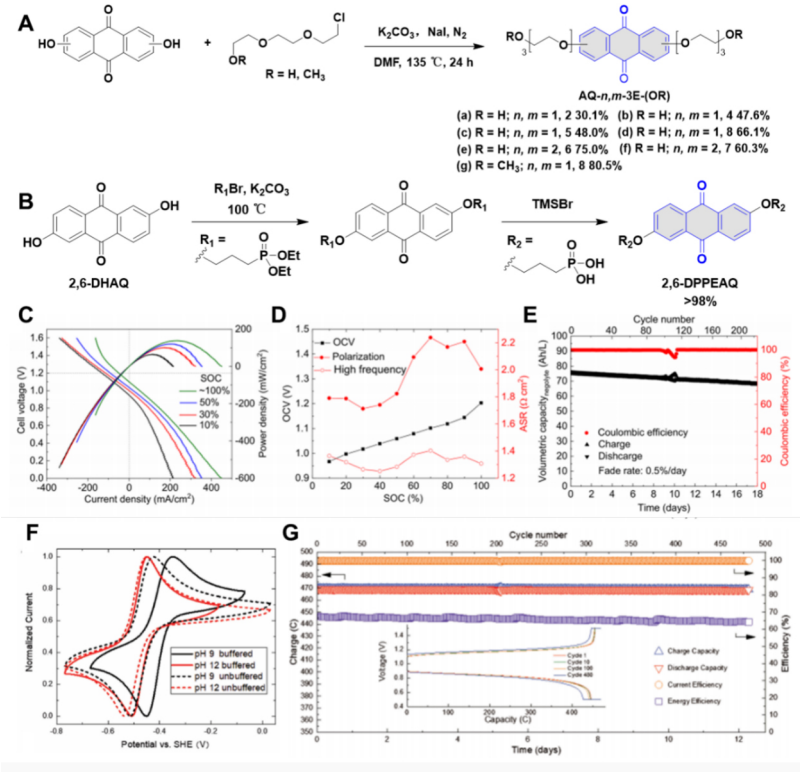

Figure 7. AQ-based derivatives and the performance for AORFBs[50,51]. (A) Synthesis of *n, m*-di-Pegylated AQ; (B) Synthesis of 2,6-DPPEAQ; (C) Battery voltage and power density *vs.* current density at 10%, 30%, 50%, and ~100% SOC. Reproduced with permission[50]. Copyright 2019, American Chemical Society; (D) OCV, high frequency, and polarization ASR versus SOC; (E) Current efficiency and charge-discharge capacities versus time and cycle number; (F) CV curves of 1 mM 2,6-DPPEAQ at pH 9 buffered solution (black solid), pH 12 buffered solution (red solid), pH 9 unbuffered solution (black dash), and pH 12 unbuffered solution (red dash). Scan rate: 100 mV s^{-1}; (G) CE (circles), energy efficiency (squares), charge (upward-pointing triangles) capacity, and discharge (downward-pointing triangles) capacity versus time and cycle number. Inset: capacity versus battery voltage at the 1st, the 10th, the 100th, and the 480th cycle. Reproduced with permission[51]. Copyright 2019, Wiley-VCH.

predicted a theoretical OCV of 0.865 V for $AQDS(NH_4)_2/NH_4I$ combination [Table 1]. When paired with the highly soluble NH_4I catholyte, the resulting AORFB displayed outstanding cycling stability over 300 cycles and the overpotential remained the same from cycle 10 to cycle 300, suggesting that the membrane and other components of the cell have good chemical compatibility without ohmic loss [Figure 8E and Table 1]. Combining with the highly soluble cathode opens a new avenue to develop pH-neutral, benign, and stable cycling AORFBs, utilizing AQ compounds promising low-cost and sustainable green energy storage.

Then, In 2020, Jiang *et al.* designed an AQ-based AORFB by using the micellization strategy [Figure 8B][53]. With a similar synthesis procedure, PEG3-, PEG12-, and PEG45-AQ micellizations were easily afforded. The CV curve confirmed that the redox pair of PEG12-AQ was completely reversible with a reduction redox potential of -0.64 V *vs.* Ag/AgCl, and when matched with $K_4Fe(CN)_6$ catholyte, it possessed an OCV of 0.9 V when combined with potassium ferrocyanide [Figure 8F and Table 1]. Moreover, the higher concentration battery showed a high CE of 99.9% and a remarkable capacity retention of 99.98%/cycle at 60 mA cm^{-2} during 180 cycles, mainly due to the hyperstability of PEG12-AQ and micellization strategy [Figure 8G].

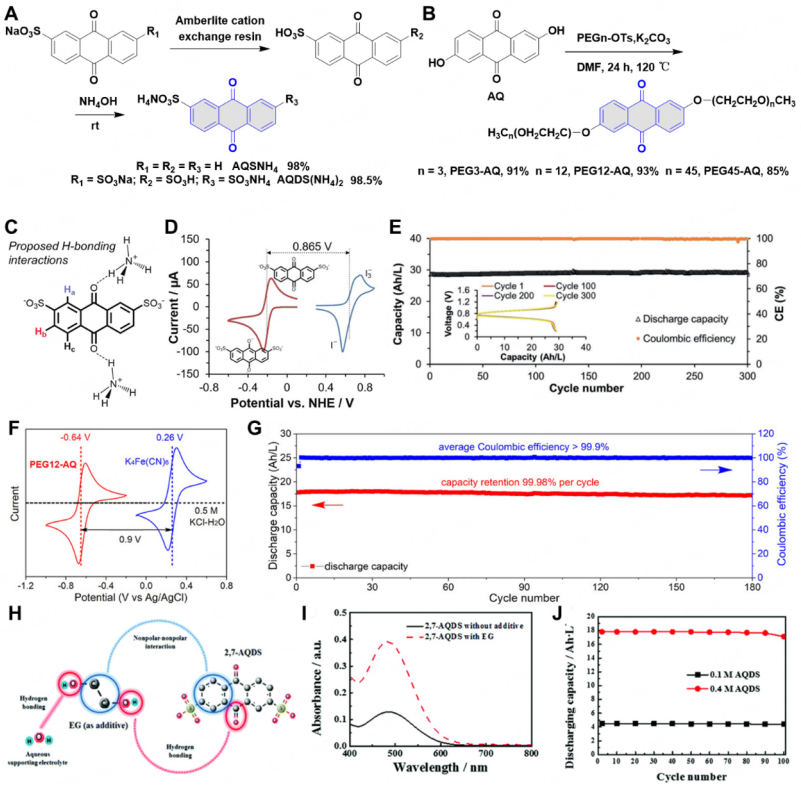

Figure 8. AQ-based derivatives and the performance for AORFBs[52,53]. (A) Synthesis of AQDS-$(NH_4)_2$; (B) Synthesis of PEG_n-AQ (n = 3, 12, 45). Reproduced with permission[52]. Copyright 2019, Wiley-VCH. (C) Schematic hydrogen bonding interactions proposed for AQDS$(NH_4)_2$; (D) CV curves for AQDS$(NH_4)_2$ and NH_4I, respectively; (E) Capacity versus cycle number for 300 cycles of 0.75 M AQDS$(NH_4)_2$/NH_4I AORFB. Current density: 60 mA cm^{-2}. Inset: selected representative voltage versus capacity profiles; (F) CV curves of PEG12-AQ (red) and $K_4Fe(CN)_6$ (blue). Conditions: 5 mM of each electrolyte in 0.5 M KCl. The dotted line was the CV curve for blank KCl. Scan rate: 50 mV s^{-1}; (G) Discharge capacity and CE of the PEG12-AQ (0.35 M)/$K_4Fe(CN)_6$ battery over 180 cycles. Current density: 60 mA cm^{-2}; (H) The scheme shows EG's role in increasing the solubility of 2,7-AQDS in an aqueous solution; (I) UV-Vis results of 2,7-AQDS dissolved in 1 M KCl with and without EG additive; (J) Discharge capacity graphs of two different AORFBs. The first AORFB used 0.3 M potassium ferrocyanide and 0.1 M 2,7-AQDS without additive at room temperature, while the second one used 1.2 M ferrocyanide containing the sodium and potassium salts of 1:1 ratio and 0.4 M 2,7-AQDS. In the second AORFB, 10 mL of 1 M EG additive was included to enhance the solubility of 2,7-AQDS in KCl. Reproduced with permission[54]. Copyright 2020, Wiley-VCH.

In the same year, Kwon *et al.* conducted an anthraquinone-2,7-disulfonic acid (2,7-AQDS) and $K_4Fe(CN)_6$ as redox couples in neutral AORFBs[54]. They succeed in enhancing the solubility of 2,7-AQDS from 0.3 to 0.8 M without any negative effects on its electrochemical performance by using an ethylene glycol (EG) additive [Figure 8I and Table 1]. It was mainly credited with the formation of the hydrogen bonds between EG additive and the electrolyte and 2,7-AQDS [Figure 8H]. Upon electrochemical testing, it was found that the AORFB with a high concentration of redox couple and 1 M EG additive had a discharge capacity of 17.8 Ah L^{-1} with 83% SOC, compared to 4.4 Ah^{-1} with 82% SOC for the AORFB with a low concentration of redox couple and no additives [Figure 8J].

In 2021, Tan *et al.* presented a new way to enable the solubility of AQ with the assistance of intramolecular H-bonds and quaternary ammonium groups [Figure 9A][55]. The synthetic procedure of the final product was carried out via two steps. 1-chloroanthraquinone(1-CAQ) is widely used in the dye field as a cheap and available intermediate. It experienced nucleophilic substitution with 3-dimethylaminopropylamin to afford 1-DPAQ. After that, by being treated with acetonitrile and methyl chloride, 1-DAPQCl was obtained with desirable yield. In consideration of available starting materials, contracted procedure and high productivity,

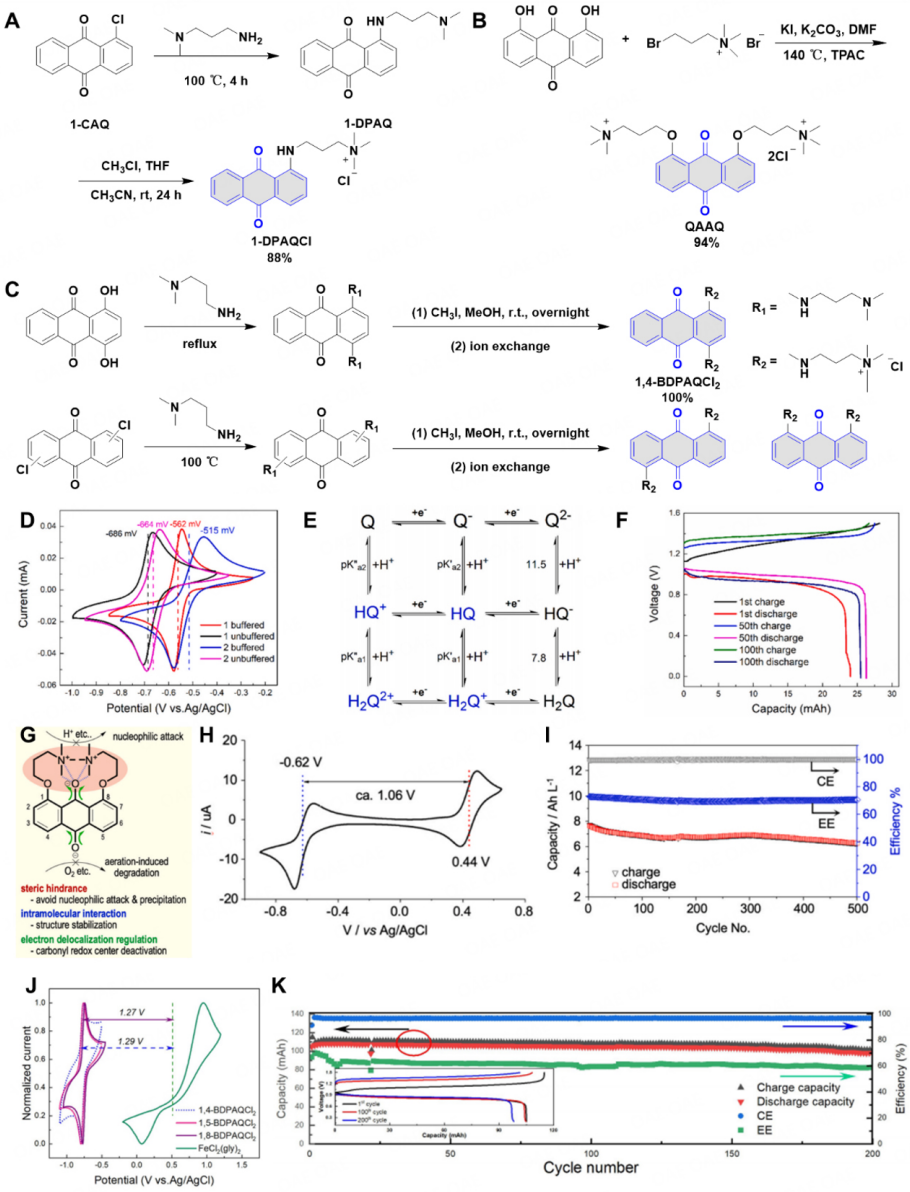

Figure 9. AQ-based derivatives and the performance for AORFBs[55-57]. (A) Synthesis of 1-DPAQCl; (B) Synthesis of QAAQ. (C) Synthesis of 1,m-BDPAQCl$_2$ (m = 4, 5, 8). Reproduced with permission[55]. Copyright 2021, Elsevier; (D) Depicts CV of 1 mM 1-DPAQCl in 1 M KCl (black) and buffered solution (red) as well as 1 mM 2-DPAQCl in 0.1 M NaCl (pink line) and buffered solution (blue). Scan rate: 50 mV s^{-1}; (E) Nine-Membered square scheme for 1-DPAQCl with electrons and protons transferred. Products marked by blue color will not exist in near neutral or alkaline unbuffered aqueous solution; (F) Charge/discharge profiles of the FcNCl/1-DPAQCl battery at 1st, 50th and 100th cycle. Reproduced with permission[56]. Copyright 2021, Elsevier; (G) Proposed strategy to enhance the stability of AQ-based molecules by combining the steric hindrance with electron delocalization regulation; (H) CV profile of 0.2 M NaCl solution containing 2 mM QAAQ and 4 mM FcNCl. Scan rate: 20 mV s^{-1}. (I) Electrochemical stability of QAAQ/FcNCl battery; (J) CV curves of 1,m-BDPAQCl$_2$ anolyte (1 mM) and the catholyte (90 mM FeCl$_2$ and 180 mM glycine) in 0.5 M KCl. Scan rate: 20 mV s^{-1}; (K) Stability for 1,8-BDPAQCl$_2$/Fe(gly)$_2$Cl$_2$ AORFB. Current density: 40 mA cm^{-2}. The inset was the voltage-capacity curves of the 1st, 100th and 200th cycles. Reproduced with permission[57]. Copyright 2022, Wiley-VCH.

1-DPAQCl is able to meet the inexpensive requirement of scalable production.

Based on the obtained AQ-based organics, it was expected that hydrophilic substitute groups at β-sites (2,3,6,7) were expected to enhance water-miscibility much better at improving solubility than α-sites (1,4,5,8). CV curves in Figure 9D showed that 1-DPAQCl had small peak-to-peak separations ΔE_p in buffered or unbuffered aqueous solution (less than 40 mV), suggesting high electrochemical reversibility and facile reaction kinetics of this molecule. It is noteworthy that there is pH movement and equilibrium in the negative solution during the charging/discharging process through the discussion of the proton transfer process [Figure 9E]. Such pH balance can ensure the long-term cycling stability of quinone-based AORFBs in neutral aqueous systems, as proved in previous works by Aziz and Gordon[51]. Significantly, an increase of 5 mV was observed in charge overpotential from 50 to 100 cycles, accompanied by a decrease in discharge overpotential at initial process of discharge [Figure 9F].

Zhao *et al.* then used a quaternary ammonium-protected AQ derivative (denoted as QAAQ) as an anolyte in AORFBs[56]. The fabrication of QAAQ concerned well-developed Williamson etherification with 8-dihydroxyanthraquinone and (3-bromopropyl) trimethylammonium bromide, then followed by a maneuverable ion-exchange step with high efficiency [Figure 9B]. By introducing armed-shaped quaternary ammonium groups, the stability of QAAQ was promoted through the synergy of steric hindrance effect and electron delocalization regulation [Figure 9G]. Upon CV profile measuring, QAAQ and FcNCl showed an OCV of 1.06 V in neutral NaCl [Figure 9H and Table 1]. When assembling a full battery with QAAQ and FcNCl, the capacity retention was 81% with corresponding CE and EE of 99% and 70%, respectively, in the 500 cycles measured [Figure 9I and Table 1].

Quinone-based pH-neutral AORFBs embody a stable electrochemical window with a voltage of ~2.5 V, which supports large space for the design of low-potential redox-active organics. However, it was still difficult to realize the ideal potential in a neutral environment for quinone derivatives, owing to intrinsic pH-dependent properties and deep energy level of the lowest unoccupied molecular orbital.

Recently, Tan *et al.* synthesized a series of quinone-based derivatives (1,4-BDPAQCl_2, 1,5-BDPAQCl_2, and 1,8-BDPAQCl_2) with low potential by bis-dimethylamino substitution, which generally consist of three steps [Figure 9C][57]. 1,8-Dichloroanthraquinone and 3-dimethylaminopropylamine were carried out to obtain 1,8-BDPAQ. Followed by dimethylation with CH_3I and the iodide/chloride ion exchange, the final product 1,8-BDPAQCl_2 was offered in high yield. 1,4-BDPAQCl_2 and 1,5-BDPAQCl_2 were obtained effectively in a similar way.

By assembling an AORFB based on 0.4 M 1,8-BDPAQCl_2 anolyte and 0.9 M $Fe(gly)_2Cl_2$ catholyte, the theoretical potential of the redox couple was measured as up to 1.29 V [Figure 9J and Table 1]. It possessed good reversibility with a redox potential of -0.755 V (*vs.* NHE) [Table 1]. Furthermore, during the operation of the aforementioned AORFB, the mean values of CE and EE were 96.6% and 61.3%, respectively. Remarkably, the capacity decay reached 0.048%/cycle and 0.88%/day over 200 cycles [Figure 9K and Table 1].

Other compounds anolytes

Bipolar molecular-based symmetric AORFBs

In 2016, bipolar organic molecules were first developed as redox-active materials for AORFBs by Winsberg and co-workers[58]. They combined 2,2,6,6-tetramethylpiperidinyl-N-oxyl and phenazine via TEG linkers, as a solubilizing functional group, to afford a redox-active organic for AORFB applications. The synthesis route is distinguished by low costs with the utilization of raw materials and simple procedure [Figure 10A]. TEG linkers were first tosylated to promote nucleophilic substitutions of phenazine alkoxides and TEMPO.

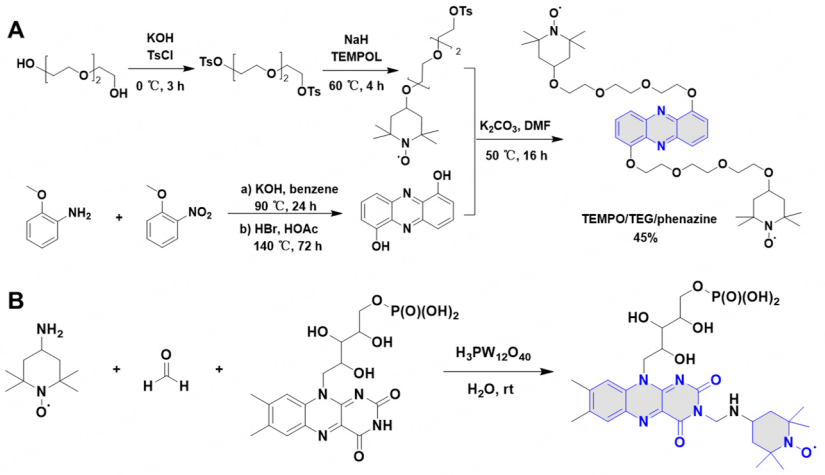

Figure 10. Designed bipolar molecular-based derivatives. (A) Synthesis of TEMPO/Phenazine combi-molecule; (B) Schematic representation of the synthesis scheme for RIBOTEMPO combi-molecule.

4-HO-TEMPO was then deprotonated with NaH and added to an excess of di-Ts-TEG to produce 2-[(2-(2-((2,2,6,6-tetramethylpiperidin-N-oxyl)ethoxy)ethoxy]ethyl 4-methylbenzenesulfonate. The synthesis of dimethoxy phenazine can be made by a Wohl-Aue reaction. The colature was afterward heated in HCl to get dihydroxyphenazine, which can be easily deprotonated with K_2CO_3 and etherified with 2-[2-(2-((2,2,6,6-tetramethylpiperidin-N-oxyl)ethoxy)ethoxy]ethyl 4-methylbenzenesulfonate, generating the bipolar TEMPO/TEG/Phenazine combi-molecule. The TEG linkages between the TEMPO and phenazine units endowed the reversible reduction/oxidation process.

TEMPO/TEG/phenazine combi-molecule based symmetric AORFB featured an OCV of 1.2 V [Figure 11A and Table 1]. According to the electrochemical performance at different current densities shown in Figure 11B, the battery capacity can reach 60% of the theoretical value. Furthermore, upon long-term galvanostatic charge-discharge cycle testing, the battery revealed CE of up to 98.3% after 1800 consecutive charge/discharge cycles [Figure 11B and Table 1]. However, the EE is only ~50% [Figure 11C, inset], which may be due to the restricted reaction kinetics of the phenazine substructure.

Later, in 2021, Shao *et al.* reported a combi-molecule, Riboflavin-TEMPO (RIBOTEMPO), with bifunctional behaviors, as it was evident from Figure 10B that the RIBOTEMPO combi-molecule could be synthesized through the Mannich reaction[59].

As a bipolar molecule, RIBOTEMPO combi-molecule could be used in both anolyte and catholyte [Figure 11D]. Upon assembling the symmetric AORFB based on the molecule above, it demonstrated an ideal OCV of 1.23 V [Figure 11E and Table 1]. Unfortunately, the cyclic stability of this molecule remained to be enhanced. According to electrochemical charge-discharge cycling, the battery indicated a capacity decay rate of 78% compared with the initial value (1655.4 mAh) and a CE of only 80% after 100 cycles [Figure 11F and G]. In order to find out the source of the decline, the electrolytes used were tested and the result revealed that the decomposition of the RIBOTEMPO combi-molecule was responsible for the capacity loss [Figure 11F and G].

These bipolar organics featured a delocalized π-electron distribution and reversible oxidation/reduction process. An ideal bipolar redox-active material is capable of gaining and losing electrons in equal quantities.

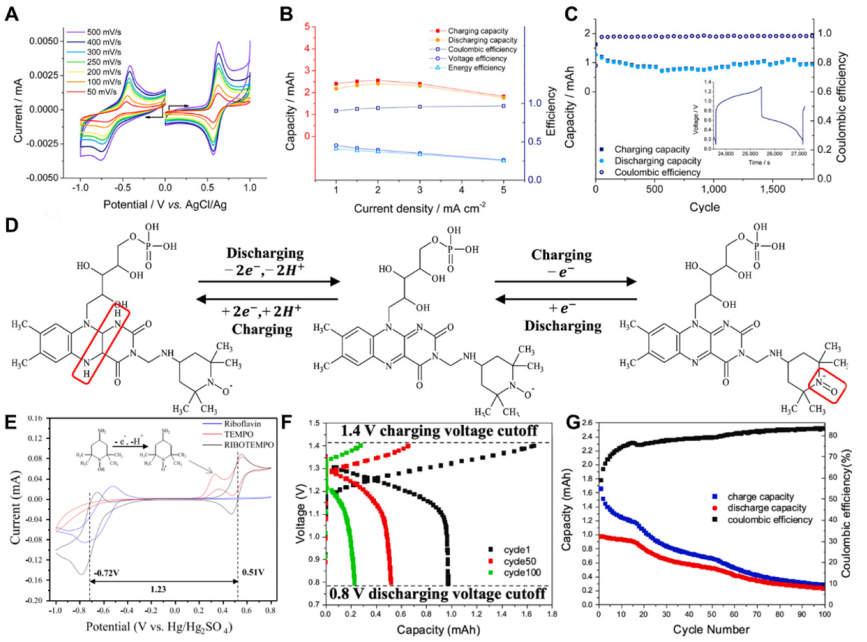

Figure 11. Performance of bipolar molecular-based symmetric AORFBs[58,59]. (A) CV curves of TEMPO/Phenazine combi-molecule in 0.1 M NaCl. Scan rate: 50-500 mV s^{-1}; (B) Electrical performance is determined by applying different current densities and the resulting capacities and efficiencies; (C) Long-term battery cycling. Inset: exemplary charge/discharge potential curve at 1 mA cm^{-2}. Condition: 10 mM combi-molecule in 0.5 M NaCl and 10 vol % diglyme. Current density: 4 mA cm^{-2}. Reproduced with permission[58]. Copyright 2016, American Chemistry Society; (D) Redox mechanism of RIBOTEMPO; (E) CV profiles of Riboflavin, TEMPO, and RIBOTEMPO in 0.1 M NaCl. Scan rate: 50 mV s^{-1}; (F,G) Demonstration of battery performance of 3 mM combined RIBOTEMPO, exhibiting galvanostatic charge/discharge profiles during the 1st, 50th, and 100th cycles as well as cycling performances and CEs. Cut-off voltage: 0.8-1.4 V. Current density: 2.5 mA cm^{-2}. Reproduced with permission[59]. Copyright 2021, Elsevier.

Unfortunately, the voltage between these two redox reactions was often > 1.6 V, which exceeded the water potential window. Hence, these molecules are highly dependent on organic solvents, which leads to lower current ratings, higher costs and environmental problems that hinder their further development[58].

Polysulfide-based AORFBs

In 2016, Wang *et al.* reported an AORFB applying polysulfide redox couple as the anolyte and $[Fe(CN)_6]^{4-}$/$[Fe(CN)_6]^{3-}$ redox pair as the catholyte based on their high solubility[60]. During the charge process, S_4^{2-} was reduced to S_2^{2-} at the negative electrode and $[Fe(CN)_6]^{4-}$ was oxidized to $[Fe(CN)_6]^{3-}$ at the positive electrode. During the discharge process, the reactions were reversed [Figure 12A]. The efficiency of assembled Fe/S batteries at different current densities from 10 to 50 mA cm^{-2} is shown in Figure 12B. Remarkable performance of the battery was achieved with CE of 99%, EE of ~74%, and capacity retention of 98% over 100 cycles [Figure 12C and Table 1]. However, there were some challenges with the design of the battery. One obvious challenge was the power density, possibly limited by the sluggish kinetics of redox reactions and the low electrical conductivity of neutral solution. These shortages can be addressed with catalysts and supporting electrolytes (e.g., NaCl) to decrease the resistivity of the electrolytes.

Thereafter, in 2021, Long *et al.* conducted further research on this system, in which they used K_2S and $K_3[Fe(CN)_6]$ as the anolyte and catholyte, respectively[61]. CV curve of 0.1 M K_2S showed a quasi-reversible redox behavior in 1.0 M KCl at 50 mV s^{-1} with potential varying from -1.3 to 0.3 V [Figure 12D]. Furthermore, battery stacks with different concentrations were constructed and investigated in the verification of practical applications [Figure 12E]. The stack with a 20.0 L 0.2 M $K_3[Fe(CN)_6]$ catholyte and a

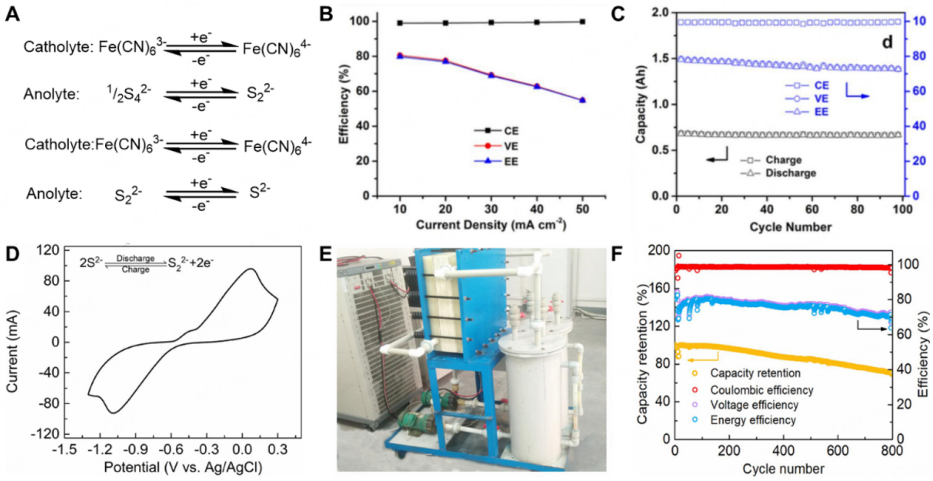

Figure 12. Polysulfide-based AORFBs[60,61]. (A) Redox mechanisms; (B) Battery efficiencies with respect to current density; (C) Cycling capacity and efficiencies with respect to cycle number. Reproduced with permission[60]. Copyright 2015, The Electrochemical Society; (D) CV curves of sulfide/polysulfide in 1.0 M KCl. Scan rate: 50 mV s^{-1}; (E) A photograph of the battery stack employing $K_3[Fe(CN)_6]$/K_2S; (F) Battery performance of the stack consisting of a 20.0 L 0.2 M $K_3[Fe(CN)_6]^+$ 1.0 M KCl as catholyte and a 20.0 L 1.0 M K_2S+1.0 M KCl as anolyte under 34 A.

20.0 L 1.0 M K_2S anolyte presented stable stability with a high capacity retention rate of 99.979%/cycle [Figure 12F and Table 1].

Azobenzene-based AORFBs

Azo compounds are regarded as viable alternatives for redox-active materials in AORFBs due to their affordability, proved stability, and capacity for two-electron transfer redox processes. In 2020, Yu *et al.* reported azobenzene-based derivatives with water-soluble groups as novel redox-active organics for AORFBs based on the redox reversibility of azo core structure. Figure 13A shows the molecular structures of corresponding azobenzene-based derivatives[40]. As an anolyte material, 4-amino-1,1'-azobenzene-3,4'-disulfonic acid monosodium salt (AADA) possessed high solubility. Furthermore, by introducing the hydrogen bond interactions using urea as a hydrotropic additive, AADA-based electrolytes could exhibit solution stability at high concentrations during a long-term cycle. In order to find out the dissolution behavior of azobenzene-based derivatives in an aqueous system, the corresponding solvation energy analyses were conducted by DFT simulations [Figure 13B]. Comparing the results, it was not hard to find that the asymmetric charge distribution can provide strong preferential solvation sites. The LSV curves demonstrated obvious plateaus, indicating that the limiting currents were diffusion-controlled [Figure 13C]. Moreover, the color of the anolyte changed from red to yellow gradually during the charging process and then back to the initial color after discharging. Additionally, the same UV-visible spectrum as the original AADA solute was observed at the end of the discharge, indicating reversible molecular changes [Figure 13D]. In combination with the ferro/ferrocyanide catholyte, the electrochemical profiles of AADA-based anolyte showed satisfactory long-term stability. In a static mode, the 0.1 M AADA-based battery showed a good capacity utilization of 81% after 700 cycles with a capacity decay rate of 0.03%/cycle and CE of ~99.7% [Figure 13E]. Furthermore, upon charge/discharge cycling test utilizing 0.5 M AADA as an anolyte with current density ranging from 10 to 40 mA cm^{-2}, the full cell presented an outstanding rate performance with a high capacity retention of 92% and a high CE of over 98% at 20 mA cm^{-2} [Figure 13F]. The corresponding discharge capacity remained approximately 76% at 20 mA cm^{-2} over 500 cycles [Figure 13G].

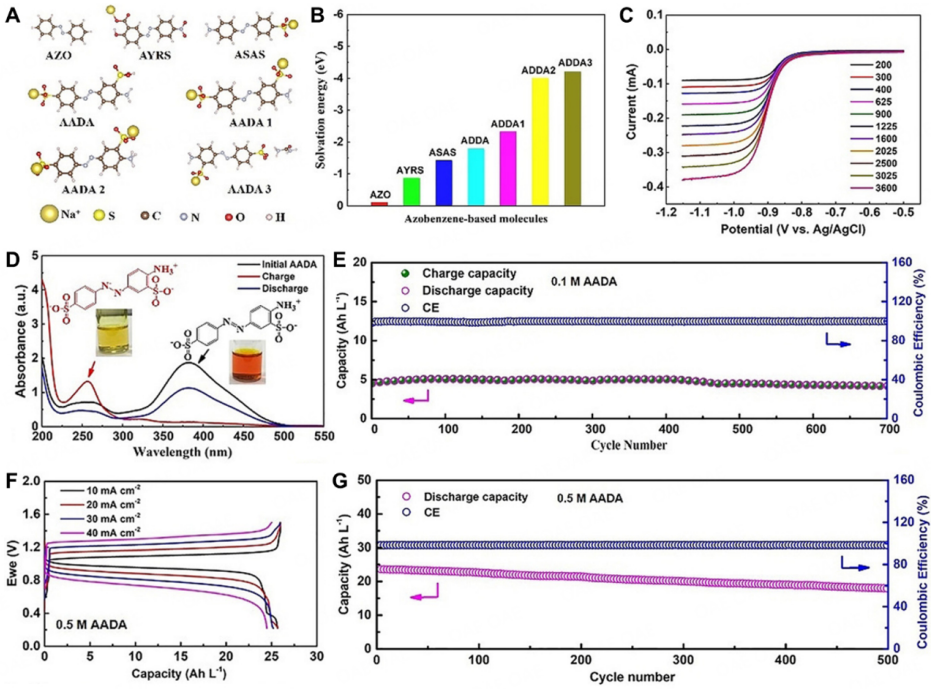

Figure 13. Performance for azobenzene-based AORFBs[40]. (A) Molecular structures of different azobenzene-based derivatives; (B) Calculated solvation energy; (C) LSV study. Condition: 5 mM AADA in 2 M NaOH. Scan rate: 5 mV s^{-1}. Rotation rates: 200-3,600 rpm; (D) UV-Vis spectra of the AADA anolyte at different redox states; (E) Cycling capacity and CE of the battery based on 0.1 M AADA. Current density: 30 mA cm^{-2}; (F) Galvanostatic charge/discharge profiles of the battery with 0.5 M AADA anolyte. Current densities: 10-40 mA cm^{-2}; (G) Cycling capacity and CE based on 0.5 M AADA battery. Current density: 20 mA cm^{-2}. Reproduced with permission[40]. Copyright 2020, Wiley-VCH.

CONCLUSION AND OUTLOOK

Currently, the environmentally friendly synthesis method and dependable electrochemical behaviors of neutral AORFBs show promise for practical, scalable energy storage applications. On the one hand, neutral AORFBs have demonstrated superior stability compared to acidic and alkaline AORFBs with comparable rate performance, energy efficiency, and power/energy densities. Conversely, side reactions of organic degradation and hydrogen/oxygen evolution are challenging under neutral circumstances, avoiding the imbalance of charge in electrolytes and exhibiting irreversible coulombic efficiency loss and capacity decay.

To further develop and implement neutral AORFBs, it is necessary to address several crucial factors. First, there is a need for high-potential redox organics and electrolytes. Organics must have high solubility, a strong positive or negative redox potential, rapid kinetics, high stability, and low price. The properties mentioned above influence the performance of the neutral AORFBs in terms of capacity, energy density, voltage, and cycle lifespan. High-throughput theoretical computing, organic physical investigations, and molecular engineering are effective methodologies for designing redox-active organics. The optimal electrolytes should be non-corrosive, non-flammable, low toxic, highly conductive, less viscous, and affordable. To obtain high-performance AORFBs, future research needs thoroughly investigate redox molecules' and electrolytes' physical and chemical characteristics. Second, it is required to have in-depth knowledge of the solution chemistry, electrochemistry of redox-active organics, and their corresponding electrolytes. The findings will aid in improving AORFB systems and give input for optimal molecular design. The in-situ cycling study can be utilized to identify the processes of AORFB capability fading. Due to the use of identical redox electrolytes on both sides of the battery, the half-cell test is an effective method for determining the stability of a single redox-active molecule; hence, the capacity decaying may be

increased[62].

Despite the progress made in the past decades, tremendous efforts are demanded to acquire desirable electrolytes to access practically viable non-viologen-based organic anolytes. The development of non-viologen-based organic anolytes still faces many key challenges and issues. Firstly, it is critical to improve the structural stability and electrochemical reversibility of organic electrolytes in order to increase the cycling lifespan of non-viologen-based organic anolytes. Electrolyte deterioration during charge and discharge includes both chemical and electrochemical decomposition. Moreover, a fundamental understanding of the underlying degradation mechanisms is incomplete and needs to be further developed. Secondly, the demand for practical applications and the achieved energy density are at odds with one another, increasing the electron transfer number and raising the cell voltage are feasible approaches to improve the energy density of non-viologen-based anolytes for pH-neutral AORFBs.

In addition, theoretical modeling is an efficient way to investigate the physicochemical properties of redox-active organics. The use of redox-active polymers or oligomers as electrolytes and the development of highly selective ion-conducting membranes are potential strategies for minimizing the redox organic crossover. The lack of specific ion-conductive membranes for AORFB systems has been the heel of their development.

DECLARATIONS

Authors' contributions

Prepared the manuscript: Sun H, Hu F, Jiang Z, Cui Z
Designed and revised the manuscript: Ravivarma M, Fan H, Song J, Kong D
All authors contributed to the discussion and preparation of the manuscript: Sun H, Hu F, Jiang Z, Cui Z, Ravivarma M, Fan H, Song J, Kong D

Availability of data and materials

Not applicable.

Financial support and sponsorship

This study was supported by the National Natural Science Foundation of China (Nos. 22101018, 22209130, and 22279100); Beijing Nova Program (Z211100002121126); Fundamental Research Funds for the Central Universities (buctrc202137); And the China Postdoctoral Science Foundation (No. 2022M722524).

Conflicts of Interest

All authors declared that there are no conflicts of interest.

Ethical approval and consent to participate

Not applicable.

Consent for publication

Not applicable.

Copyright

© The Author(s) 2023.

REFERENCES

1. Sawin JL, Sverrisson F, Leidreiter A. Renewable energy and sustainable development; 2016. Available from: https://www.worldfuturecouncil.org/wp-content/uploads/2016/08/WFC_2016_Renewable-Energy-and-Sustainable-Development.pdf [Last accessed on 4 Jul 2023]

2. Navalpotro P, Castillo-martínez E, Carretero-gonzález J. Sustainable materials for off-grid battery applications: advances, challenges and prospects. *Sustain Energ Fuels* 2021;5:310-31. DOI
3. Rahman A, Farrok O, Haque MM. Environmental impact of renewable energy source based electrical power plants: solar, wind, hydroelectric, biomass, geothermal, tidal, ocean, and osmotic. *Renew Sust Energ Rev* 2022;161:112279. DOI
4. Dunn B, Kamath H, Tarascon JM. Electrical energy storage for the grid: a battery of choices. *Science* 2011;334:928-35. DOI PubMed
5. Wang W, Luo Q, Li B, Wei X, Li L, Yang Z. Recent progress in redox flow battery research and development. *Adv Funct Mater* 2013;23:970-86. DOI
6. Li G, Lou X, Peng C, Liu C, Chen W. Interface chemistry for sodium metal anodes/batteries: a review. *Chem Synth* 2022;2:16. DOI
7. Zhang L, Hu X, Wang Z, et al. Hybrid electrochemical energy storage systems: an overview for smart grid and electrified vehicle applications. *Renew Sust Energ Rev* 2021;139:110581. DOI
8. Kebede AA, Kalogiannis T, Van Mierlo J, Berecibar M. A comprehensive review of stationary energy storage devices for large scale renewable energy sources grid integration. *Renew Sust Energ Rev* 2022;159:112213. DOI
9. Liu W, Lu W, Zhang H, Li X. Aqueous flow batteries: research and development. *Chemistry* 2019;25:1649-64. DOI
10. Yao X. Boosting lithium-selenium batteries. *Chem Synth* 2022;2:10. DOI
11. Thaller LH. Electrically rechargeable redox flow cells. Available from: https://patents.google.com/patent/US3996064A/en [Last accessed on 4 Jul 2023]
12. Iwakiri I, Antunes T, Almeida H, Sousa JP, Figueira RB, Mendes A. Redox flow batteries: materials, design and prospects. *Energies* 2021;14:5643. DOI
13. Park M, Ryu J, Wang W, Cho J. Material design and engineering of next-generation flow-battery technologies. *Nat Rev Mater* 2017:2. DOI
14. Kamat PV, Schanze KS, Buriak JM. Redox flow batteries. *ACS Energy Lett* 2017;2:1368-9. DOI
15. Chen Q, Lv Y, Yuan Z, et al. Organic electrolytes for pH-neutral aqueous organic redox flow batteries. *Adv Mater* 2021;32:2108777. DOI
16. Li Z, Lu YC. Material design of aqueous redox flow batteries: fundamental challenges and mitigation strategies. *Adv Mater* 2020;32:e2002132. DOI PubMed
17. Luo J, Hu B, Hu M, Zhao Y, Liu TL. Status and prospects of organic redox flow batteries toward sustainable energy storage. *ACS Energy Lett* 2019;4:2220-40. DOI
18. Huskinson B, Marshak MP, Suh C, et al. A metal-free organic-inorganic aqueous flow battery. *Nature* 2014;505:195-8. DOI
19. Lin K, Chen Q, Gerhardt MR, et al. Alkaline quinone flow battery. *Science* 2015;349:1529-32. DOI
20. Feng R, Zhang X, Murugesan V, et al. Reversible ketone hydrogenation and dehydrogenation for aqueous organic redox flow batteries. *Science* 2021;372:836-40. DOI
21. Hu B, DeBruler C, Rhodes Z, Liu TL. Long-cycling aqueous organic redox flow battery (AORFB) toward sustainable and safe energy storage. *J Am Chem Soc* 2017;139:1207-14. DOI PubMed
22. Liu T, Wei X, Nie Z, Sprenkle V, Wang W. A total organic aqueous redox flow battery employing a low cost and sustainable methyl viologen anolyte and 4-HO-TEMPO catholyte. *Adv Energy Mater* 2016;6:1501449. DOI
23. Pan F, Wang Q. Redox species of redox flow batteries: a review. *Molecules* 2015;20:20499-517. DOI PubMed PMC
24. Cao J, Tian J, Xu J, Wang Y. Organic flow batteries: recent progress and perspectives. *Energy Fuels* 2020;34:13384-411. DOI
25. Kwabi DG, Ji Y, Aziz MJ. Electrolyte lifetime in aqueous organic redox flow batteries: a critical review. *Chem Rev* 2020;120:6467-89. DOI PubMed
26. Beh ES, De Porcellinis D, Gracia RL, Xia KT, Gordon RG, Aziz MJ. A neutral pH aqueous organic-organometallic redox flow battery with extremely high capacity retention. *ACS Energy Lett* 2017;2:639-44. DOI
27. Jing Y, Zhao EW, Goulet MA, et al. In situ electrochemical recomposition of decomposed redox-active species in aqueous organic flow batteries. *Nat Chem* 2022;14:1103-9. DOI
28. Debruler C, Hu B, Moss J, et al. Designer two-electron storage viologen anolyte materials for neutral aqueous organic redox flow batteries. *Chem* 2017;3:961-78. DOI
29. Li H, Fan H, Hu B, Hu L, Chang G, Song J. Spatial structure regulation: a rod-shaped viologen enables long lifetime in aqueous redox flow batteries. *Angew Chem Int Ed Engl* 2021;60:26971-7. DOI PubMed
30. Hu S, Li T, Huang M, et al. Phenylene-bridged bispyridinium with high capacity and stability for aqueous flow batteries. *Adv Mater* 2021;33:e2005839. DOI
31. Lin K, Gómez-bombarelli R, Beh ES, et al. A redox-flow battery with an alloxazine-based organic electrolyte. *Nat Energy* 2016:1. DOI
32. Hollas A, Wei X, Murugesan V, et al. A biomimetic high-capacity phenazine-based anolyte for aqueous organic redox flow batteries. *Nat Energy* 2018;3:508-14. DOI
33. Orita A, Verde MG, Sakai M, Meng YS. A biomimetic redox flow battery based on flavin mononucleotide. *Nat Commun* 2016;7:13230. DOI PubMed PMC
34. Li H, Fan H, Ravivarma M, Hu B, Feng Y, Song J. A stable organic dye catholyte for long-life aqueous flow batteries. *Chem Commun* 2020;56:13824-7. DOI
35. Fan H, Zhang J, Ravivarma M, et al. Radical charge population and energy: critical role in redox potential and cycling life of piperidine nitroxyl radical cathodes in aqueous zinc hybrid flow batteries. *ACS Appl Mater Interfaces* 2020;12:43568-75. DOI

36. Hu B, Fan H, Li H, Ravivarma M, Song J. Five-membered ring nitroxide radical: a new class of high-potential, stable catholytes for neutral aqueous organic redox flow batteries. *Adv Funct Mater* 2021;31:2102734. DOI
37. Liu Y, Goulet M, Tong L, et al. A long-lifetime all-organic aqueous flow battery utilizing TMAP-TEMPO radical. *Chem* 2019;5:1861-70. DOI
38. Fan H, Hu B, Li H, Ravivarma M, Feng Y, Song J. Conjugate-driven electron density delocalization of piperidine nitroxyl radical for stable aqueous zinc hybrid flow batteries. *Angew Chem Int Ed Engl* 2022;61:e202115908. DOI PubMed
39. Fan H, Wu W, Ravivarma M, et al. Mitigating ring-opening to develop stable TEMPO catholytes for pH-neutral all-organic redox flow batteries. *Adv Funct Materials* 2022;32:2203032. DOI
40. Zu X, Zhang L, Qian Y, Zhang C, Yu G. Molecular engineering of azobenzene-based anolytes towards high-capacity aqueous redox flow batteries. *Angew Chem Int Ed Engl* 2020;59:22163-70. DOI
41. Pang S, Wang X, Wang P, Ji Y. Biomimetic Amino acid functionalized phenazine flow batteries with long lifetime at near-neutral pH. *Angew Chem Int Ed Engl* 2021;60:5289-98. DOI
42. Xu J, Pang S, Wang X, Wang P, Ji Y. Ultrastable aqueous phenazine flow batteries with high capacity operated at elevated temperatures. *Joule* 2021;5:2437-49. DOI
43. Huang J, Hu S, Yuan X, et al. Radical stabilization of a tripyridinium-triazine molecule enables reversible storage of multiple electrons. *Angew Chem Int Ed Engl* 2021;60:20921-5. DOI
44. Wiberg C, Evenäs L, Busch M, Ahlberg E. Naphthalene diimides (NDI) in highly stable pH-neutral aqueous organic redox flow batteries. *J Electroanal Chem* 2021;896:115224. DOI
45. Wiberg C, Owusu F, Wang E, Ahlberg E. Electrochemical evaluation of a napthalene diimide derivative for potential application in aqueous organic redox flow batteries. *Energy Technol* 2019;7:1900843. DOI
46. Medabalmi V, Sundararajan M, Singh V, Baik M, Byon HR. Naphthalene diimide as a two-electron anolyte for aqueous and neutral pH redox flow batteries. *J Mater Chem A* 2020;8:11218-23. DOI
47. Pinheiro D, Pineiro M, de Melo JSS. Sulfonated tryptanthrin anolyte increases performance in pH neutral aqueous redox flow batteries. *Commun Chem* 2021;4:89. DOI PubMed PMC
48. Hu P, Lan H, Wang X, et al. Renewable-lawsone-based sustainable and high-voltage aqueous flow battery. *Energy Storage Mater* 2019;19:62-8. DOI
49. Li Z, Jiang T, Ali M, Wu C, Chen W. Recent progress in organic species for redox flow batteries. *Energy Storage Mater* 2022;50:105-38. DOI
50. Jin S, Jing Y, Kwabi DG, et al. A Water-miscible quinone flow battery with high volumetric capacity and energy density. *ACS Energy Lett* 2019;4:1342-8. DOI
51. Ji Y, Goulet M, Pollack DA, et al. A phosphonate-functionalized quinone redox flow battery at near-neutral pH with record capacity retention rate. *Adv Energy Mater* 2019;9:1900039. DOI
52. Hu B, Luo J, Hu M, Yuan B, Liu TL. A pH-neutral, metal-free aqueous organic redox flow battery employing an ammonium anthraquinone anolyte. *Angew Chem Int Ed Engl* 2019;58:16629-36. DOI PubMed
53. Chai J, Wang X, Lashgari A, Williams CK, Jiang JJ. A pH-neutral, aqueous redox flow battery with a 3,600-cycle lifetime: micellization-enabled high stability and crossover suppression. *ChemSusChem* 2020;13:4069-77. DOI PubMed
54. Lee W, Permatasari A, Kwon Y. Neutral pH aqueous redox flow batteries using an anthraquinone-ferrocyanide redox couple. *J Mater Chem C* 2020;8:5727-31. DOI
55. Xia L, Huo W, Gao H, et al. Intramolecular hydrogen bonds induced high solubility for efficient and stable anthraquinone based neutral aqueous organic redox flow batteries. *Jops* 2021;498:229896. DOI
56. Zhu Y, Li Y, Qian Y, et al. Anthraquinone-based anode material for aqueous redox flow batteries operating in nondemanding atmosphere. *J Power Sources* 2021;501:229984. DOI
57. Xia L, Zhang Y, Wang F, et al. A low-potential and stable bis-dimethylamino-substituted anthraquinone for ph-neutral aqueous redox flow batteries. *ChemElectroChem* 2022:9. DOI
58. Winsberg J, Stolze C, Muench S, Liedl F, Hager MD, Schubert US. TEMPO/phenazine combi-molecule: a redox-active material for symmetric aqueous redox-flow batteries. *ACS Energy Lett* 2016;1:976-80. DOI
59. Nambafu GS, Siddharth K, Zhang C, et al. An organic bifunctional redox active material for symmetric aqueous redox flow battery. *Nano Energy* 2021;89:106422. DOI
60. Wei X, Xia G, Kirby B, et al. An aqueous redox flow battery based on neutral alkali metal ferri/ferrocyanide and polysulfide electrolytes. *J Electrochem Soc* 2016;163:A5150-3. DOI
61. Long Y, Xu Z, Wang G, et al. A neutral polysulfide/ferricyanide redox flow battery. *iScience* 2021;24:103157. DOI PubMed PMC
62. Wiberg C, Busch M, Evenäs L, Ahlberg E. The electrochemical response of core-functionalized naphthalene Diimides (NDI) - a combined computational and experimental investigation. *Electrochimica Acta* 2021;367:137480. DOI